Thermal effects on solar radiated sand surfaces containing landmines—a heat transfer analysis

Stefan Sjökvist[1,2,3], Mikael Georgson[2], Stefan Ringberg[2], Magnus Uppsäll[2] and Dan Loyd[3]

[1] Department of Military Technology, National Defence College, P.O. Box 27805, SE-115 93 Stockholm, Sweden

[2] Department of IR-System, Defence Research Establishment, P.O. Box 1165, SE-581 11 Linköping, Sweden

[3] Division of Applied Thermodynamics and Fluid Mechanics, Linköping University, SE-581 83 Linköping, Sweden

Abstract

This paper reports on the possibility of modelling thermal effects for detecting mines using infrared imaging systems. Results from experiments made in an indoor test landscape, using a sandbox and a solar panel with measuring instruments, are compared to simulated data from a heat transfer model. The radiation from the panel was varied in order to resemble the solar variation from sunrise to sunset. The different temperatures of the sand surface, the sand at different depths and on the surfaces of the four generic mines were sampled at one-minute intervals throughout the experiments. Infrared cameras working in the 2-5 µm and 8-12 µm bands were used in order to record images of the sand surface. The camera system calculates the apparent temperature of selected areas of the images based on the detected radiation. The simulation was carried out using the Finite Element Method.

The sequences of the infrared images show the variation in emitted radiation as the irradiation of the surface is varied. There are two different phenomenon dominating the two wavelength bands. In 2-5 µm region there is a reflecting dominance and in the 8-12 µm region the radiation originates mainly from emission. The simulation shows good agreement with the experimental result for the depth profile, where the temperatures were studied along a vertical line through the centre of the mine, as well as for the surface temperature.

1   Introduction

Around the world there is a growing interest in reducing the usage of mines and to clear existing mine fields, both areas having its own specific problems to overcome. The mine detection procedure is complicated as the signals that indicate the presence of mines can originate from numerous objects apart from mines, e.g. rocks, roots, splinters, surface roughness and grass vegetation. These effects can also be a contributing factor to why mines do not show the expected signals. Different groups are working with different techniques in order to find individual mines or minefields. To cover most situations, the most likely detection system is a combination of two or more methods as each technique have its own advantages and disadvantages. A multi sensor system could reduce the false alarm rate due to variations of the ground and weather conditions. Most of the techniques concentrate on single mines e.g. ground penetrating radar, metal detectors and biological sensors, see Christiansen and Ringberg [1]. These techniques require detectors mounted on vehicles or man carried equipment. An airborne infrared system could be used in order to cover large areas in a short time in order to find minefields rather than single mines. Surface laid mines could be detected owing to different solar absorption properties to the surrounding, whereas buried mines could even be detected due to secondary effects such as dig marks and disturbed vegetation.

This paper reports on the possibility of a numerical model to predict thermal effects for detecting mines using infrared imaging systems. Results from experiments made in an indoor test landscape, using a sandbox with a solar panel and measuring instruments, are compared to simulated data from a heat transfer model.

2   Experiment

The experiments were carried out in an indoor test landscape with a partly insulated sandbox containing pure dry sand and with the dimensions $1m \times 1m \times 0.4m$, see figure 1. The solar panel has 64 light bulbs, each with a spectral distribution similar to the sun, this means that the main part of the radiation is between $0.3-3$ μm. The intensity from the solar panel above the sandbox varied linearly in time, from zero to full scale in steps. The full-scale reading gave approximately 600 W/m^2 on the surface of the sandbox. The intensity was increased every fifteen minutes, reaching maximum level after 2 h 45 min. Maximum intensity was hold for 1 hour

and then followed by a decrease in intensity in the same way as the increase. The four test mines, see figure 2, were from the left, (1) beeswax only (without casing), (2) a genuine antipersonnel mine filled with wax with similar thermal properties as real trotyl (TNT). The body is made of phenolic plastic covered with rubber, (3) wax only (without casing), and (4) an aluminium casing filled with wax. All mines were cylindrical with a diameter of 8 cm, the aluminium cased mine had a diameter of 9 cm. The thickness was roughly 3 cm. The distances between the centre of the test mines were 20 centimetres.

A high-performance logger system based on Pt-100 probes was used to record the temperature of the mines and the sand. The probes were attached to the centre of the mines on the upper side as well as on the underside. The generic mines were covered with approximately 3 mm of sand making no part of the mines visible in order to avoid effects from different emissivity for the background and the generic mines. Two probes were recording the sand temperature. One of the probes were buried at a depth of 30 cm and the other probe at 5cm from the edge of the antipersonnel mine at the same depth as the top probes attached to the mines. Two probes were recording the air-temperature above the sandbox and outside the radiation from the solar panel. The temperatures were logged every minute during 24 hours. Simultaneously with the logger system an Agema Thermovision 900 system were recording infrared images of the buried mine-signatures, at a speed of one image per minute. The infrared cameras were mounted in the centre of the solar panel 2.1 m above the sand surface and fitted with $20°$ lenses. Images of the sand surface were recorded during 24 hours. Some infrared images are shown in appendix 1.
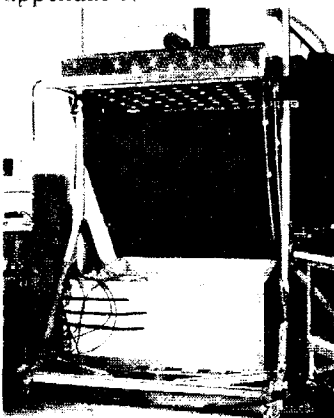

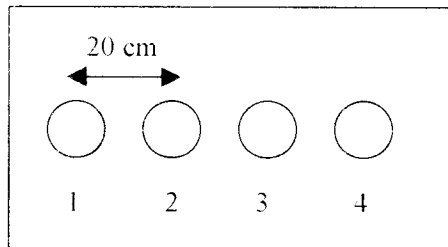Figure 1. The sandbox and its solar panel.

Figure 2. Placing of the generic mines.

3   Heat Transfer Equations

The temperature field of the considered insulated sandbox and the mine can be solved from the three-dimensional heat conduction equation and its boundary conditions, see Carslaw and Jaeger [2], and Holman [3]

The heat conduction equation in three-dimensional Cartesian space co-ordinates and time (x, y, z, t) is shown in equation (1).

$$\rho c \frac{\partial T}{\partial t} = \frac{\partial}{\partial x}\left(k_x \frac{\partial T}{\partial x}\right) + \frac{\partial}{\partial y}\left(k_y \frac{\partial T}{\partial y}\right) + \frac{\partial}{\partial z}\left(k_z \frac{\partial T}{\partial z}\right) - \dot{q} \tag{1}$$

The density, ρ, the specific heat capacity, c, and the thermal conductivity in direction i, k_i, depend on co-ordinates and temperature, and $\dot{q}$ is energy generated per unit volume, [W/m^3].

The possible boundary conditions for equation (1) are radiation, prescribed temperature, prescribed heat flux and convection heat transfer.

The free convection heat transfer boundary (index B for boundary) over the mine and its surroundings is given by equation (2).

$$k_x \frac{\partial T}{\partial x}l_x + k_y \frac{\partial T}{\partial y}l_y + k_z \frac{\partial T}{\partial z}l_z + h_b\left(T - T_{surrounding}\right) = 0 \tag{2}$$

The direction cosines are represented by l_i. The convection heat transfer coefficient for the boundary, h_B, and the surrounding temperature, $T_{surrounding}$, can vary along the boundary and with time.

The prescribed heat flux, q_B, can vary along the boundary and with time according to equation (3).

$$k_x \frac{\partial T}{\partial x}l_x + k_y \frac{\partial T}{\partial y}l_y + k_z \frac{\partial T}{\partial z}l_z + q_B = 0 \tag{3}$$

The radiation can also vary along its boundary and with time and it is written by equation (4), (ε_{12} is the resulting emissivity coefficient).

$$\dot{q}_R = \sigma \cdot \varepsilon_{12} \cdot (T^4 - (T_{surrounding})^4) \tag{4}$$

The prescribed temperature can vary along the boundary and with time, and is given by equation (5).

$$T_B = T_B(x_B, y_B, z_B, t) \tag{5}$$

4   Heat Transfer Model

The purposes of the model are mainly predicting thermal phenomenon, optimising measurements, analysis tool of collected data and study weather and soil influence. A numerical method, the finite element method, has been chosen in order to solve the different thermal conditions, see Zienkiewicz [4]. The finite element package THAFEM (Thermal and Heat Analysis by Finite Element Method) has been used, see Loyd [5].

THAFEM is a special purpose program, intended for two-dimensional and axi-symmetric problems, stationary as well as time dependent. Consideration of the possibility of phase change in the studied material can be taken. The properties of the model may vary from element to element. The material behaviour may be isotropic or anisotropic. In this study, the problem is reduced to a two-dimensional axi-symmetric problem with appropriate boundary conditions. The model, which is analysed, and the co-ordinate system, is illustrated in figure 3.
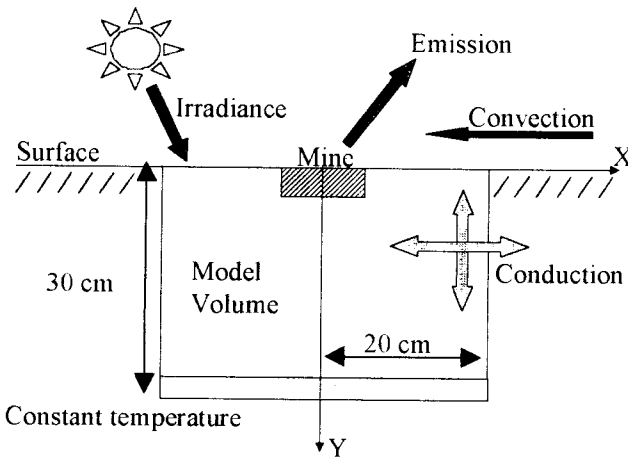
Figure 3. Co-ordinate system and the geometry of the model.

The actual set up in the finite element package THAFEM has 336 nodes. The dimensions of the model are 20 cm in the x-direction (from centre of the mine), and 30 cm in y-direction, see figure 4. The reason for these dimensions is that the influence of the mine is not interacting with the borders for the actual circumstances.

•All nodes have an initial temperature of 17°C.

182　　　Advanced Computational Methods in Heat Transfer

•The sixteen bottom nodes have the prescribed temperature of 17°C.
•The surface has a prescribed radiation heat flux. The radiation exchange with the surroundings varies in time according to measured conditions.
•The surface of the volume has a free convection heat transfer. The convective heat transfer coefficient is constant in time. but could easily be changed to be time dependent.

The temperature field was calculated for 24 hours, and compared with experimental measurements, both the logger system, based on Pt-100 probes, and the AGEMA Thermovision 900 system. For the actual properties in the FEM-model see table 1, and Sundgren [6], Accetta and Shumaker [7].

	Sand	Antipersonnel Mine
Thermal Conductivity (W/mK)	0,75	0,4
Specific Heat (kJ/kgK)	710	1120
Density (kg/m³)	1650	1350
Emissivity factor(effective)	0.2	

Table 1. Input data for the FEM-model.

THAFEM

Thermal and Heat Analysis
by Finite Element Method.
1997-11-10 14.41
My2d, peirsonmina i nivå m
ad markytan, 1 dygn. vero
MODEL PLOT
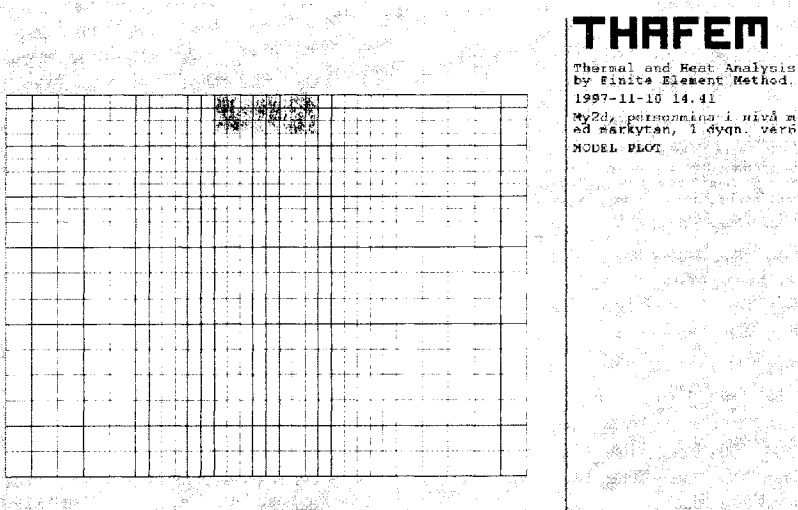
Figure 4. The axi-symmetric FEM-model and its 336 nodes.

5   Results

5.1   Verifying test and result

The results concentrate on the thermal effects according to the difference between the antipersonnel mine, and its neighbouring sand background.
The first experiment was a full-radiation test, approximately 600 W/m² radiate the surface during 4 hours, and then the solar panel was turned off. The reason was to examine the response from the logger system and from our FEM-model. The result is shown in figure 5.
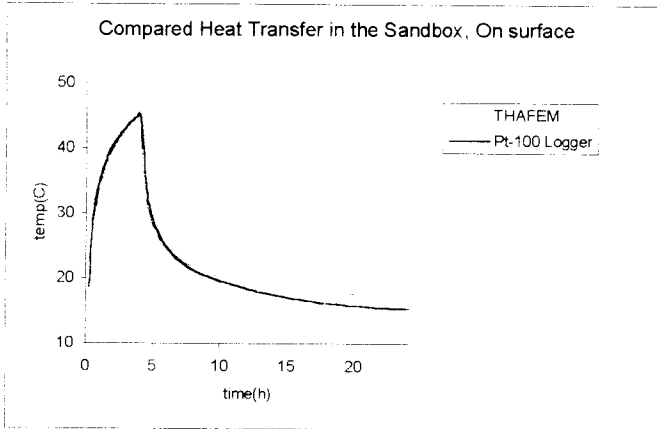
Figure 5. Surface temperature, Compared heat transfer in the sandbox between the Pt-100 probes and the FEM-model.

The two curves correspond to each other very well for the first 10 hours but then there is a small difference because the room temperature dropped to a lower level than the simulated room temperature. Similar tests were done at different depths in order to verify that the model and the Pt-100 probes showed same results. These depth results show similar agreement.

5.2   Simulation results

The next step of the analysis was to compare simulation results with the infrared imaging system results. The solar panel radiated linearly from zero to full scale in steps. The intensity was increased every fifteen minute, reaching the maximum level after 2 h 45 min. Maximum intensity was maintained for 1 hour and then decreased similarly to zero. After 16 hours, the measurement was terminated because the alterations of the temperatures were low. The interesting point is to see how well the three

different temperature-estimating methods agree and will be in accordance
to the difference between the mines and its sand background. The result of
the Pt-100 probes is shown in figure 6.
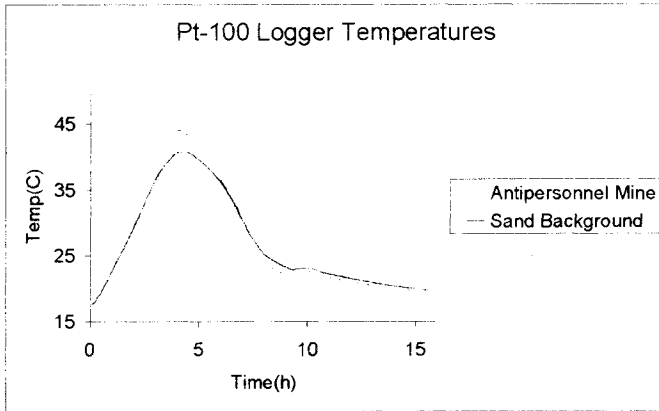
Figure 6. Surface temperature, Pt-100-probes.

The imaging system calculates the temperatures based on the assumption
that all surfaces have the same emission-coefficients. Therefore, the results
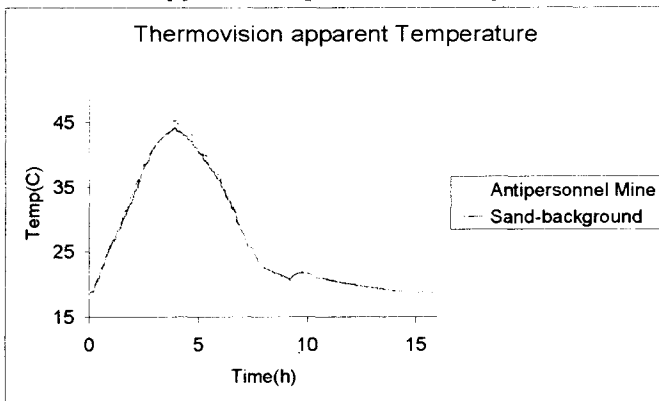are shown in apparent temperatures, see figure 7.

*Figure 7. Surface temperature, AGEMA Thermovision 900 apparent
temperature in the wavelength-band 8-12 μm.*

The curves in figure 7 indicate that there is a small contrast between the
antipersonnel mine and its background. This difference is smaller than the
difference measured by the Pt-100 probes and the calculated temperatures
in the simulation model. The temperature probes and the simulated data
show the temperatures on the top of the mine, whereas the imaging system

estimates the temperature on the sand. The results, from the simulation model, show good agreement with the other measurements, see figure 8.
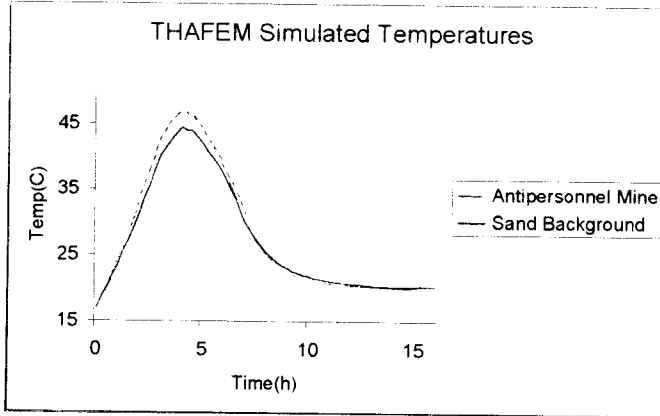
Figure 8. Surface temperature, THAFEM-simulation.

The shape of the curves in figure 8 corresponds well with the measurements, even the difference in temperature between the mine and the background corresponds well. The maximal levels of the temperatures are approximately 1,5 °C higher than the measured corresponding curves. The difference depends on the uncertainty in the input properties and differences between the experimental and the simplified boundary conditions.

Some infrared images from the laboratory indoor sandbox are shown in appendix 1. The images show the variation of the thermal signature during the artificially cycled solar radiation. From the images in appendix 1, it is clear that the mine with aluminium case, the right one, displays a bigger difference in apparent temperature to the background than the plastic antipersonnel mine, second from left.

Conclusions

The conclusion is that it is possible to make a simulation model for predicting heat transfer in sand containing land mines. The simulated data predicts the temperature variation for a dry, irradiated sand surface. The results agree well with the measurements and it shows that the simulation considers the essential parameters. The infrared images show the difference between the contrast of the rubber-covered antipersonnel mine and the aluminium cased mine, that indicates that detecting the rubber

covered antipersonnel mine is a more difficult task. However, the simulation tool provides a possibility to test different factors in simulation models of landmines, and study the possibility to detect landmines with infrared imaging technique. Preliminary studies show that there are many factors interacting with each other. For a more complex system, e g wet sand, the model has to be improved, allowing different levels of humidity.
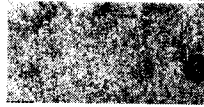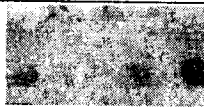
Outlook
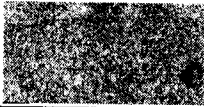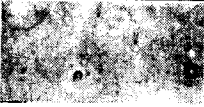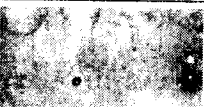
With the result in this paper as background, we will now continue with studying how different levels of water-saturation in the sand will modify the results, in infrared imaging measurements as well as in modelling and simulation.

References

[1]   Christiansen A-L and Ringberg S, *Optical Mine Reconnaissance at the National Defence Research Establishment. Multispectral Imaging and Classification:Thermodynamic Soil Modelling,* proceedings of the Eurel international conference on "The detection of abandoned land mines", Edinburgh, UK, 1996.

[2]   H. S. Carslaw and J. C. Jaeger, *Conduction of Heat in Solids,* 2nd ed., Oxford University Press, Oxford, 1959.

[3]   J. P. Holman, *Heat Transfer,* 7th ed., McGraw-Hill, London, ISBN 0-07-112644-9, 1992.

[4]   O. C. Zienkiewicz, *The Finite Element Method,* McGraw-Hill, London, 1977.

[5]   D. Loyd, G. Andersson, and M. Fröier, `THAFEM - a finite element program for heat transfer analysis`, *Finite Element Systems - A Handbook* (C. A. Brebbia, Ed.), 3 Edn, Springer - Verlag, pp. 721-732,Berlin, 1985.

[6]   J.Sundgren, *Thermal Properies of Soils and Rocks,* Swedish Geotechnical Institute, Report No35, ISSN 0348-0755, 1988.

[7]   J. S. Accetta, D. L.Shumaker, *The Infrared and Electro-Optical Systems Handbook,* SPIE Optical Engineering Press, ISBN 0-8194-1072-1, 1993

Appendix 1

Infrared Images for the generic mines, AGEMA Thermovision 900 system. For the different generic mines location, see chapter "Experiment".

	Dynamic Range	3-5μm IR-Scanner Images (Sw)	8-12μm IR-Scanner Images (Lw)
Before starting the solar panel	Sw: 617-650 Lw: 1155-1179		
1 hour after starting the solar panel	Sw: 1131-2796 Lw: 1240-1381		
2 hours after starting the solar panel	Sw: 1493-3674 Lw: 1356-1570		
3 hours after starting the solar panel	Sw: 1887-8191 Lw:1505-1780		
4 hours after starting the solar panel	Sw: 1997-8191 Lw: 1600-1866		
5 hours after starting the solar panel	Sw: 1784-3665 Lw: 1608-1756		
6 hours after starting the solar panel	Sw: 1463-2998 Lw: 1520-1618		
7 hours after starting the solar panel	Sw: 862-948 Lw: 1378-1446		
8 hours after starting the solar panel	Sw: 692-807 Lw: 1235-1336		
9 hours after starting the solar panel	Sw: 664-756 Lw: 1208-1282		